Published in final edited form as:
Cell Mol Bioeng. 2012 December 1; 5(4): 463–473. doi:10.1007/s12195-012-0242-y.

Mechanical strain controls endothelial patterning during angiogenic sprouting

Jacob Ceccarelli, **Albert Cheng**, and **Andrew J. Putnam**
Department of Biomedical Engineering, University of Michigan, Ann Arbor, 1101 Beal, Ann Arbor, MI 48109, USA

Abstract

Cyclic strain is known to affect endothelial cell phenotype, but its effects on neovascular pattern formation remain poorly understood. To examine how cyclic strain affects angiogenesis, we designed a stretchable, polydimethylsiloxane (PDMS)-based multi-well system that supports a 3D cell culture model of angiogenesis, consisting of endothelial cells coated onto microcarrier beads embedded in a fibrin gel with a supporting monolayer of smooth muscle cells atop the gel. Calibration of the integrated system showed a linear relationship between applied strain and strain within the fibrin gel. Capillaries formed in unstrained conditions grew radially outward, while 3D constructs subjected to 10% cyclic strain at 0.7 Hz sprouted in a direction parallel to the applied strain. Removal of the tissue from the strain stimulus eliminated directional sprouting. To better understand this directional biasing, the strain field surrounding a microcarrier bead was modeled computationally, showing local strain anisotropy surrounding a microcarrier. Confocal reflection microscopy revealed only modest fiber alignment in regions of the gel close to microcarriers, with no evidence of alignment further away. Together, these data showed that externally applied cyclic strain can spatially pattern capillaries in a 3D culture, and suggests a means to control pattern formation in engineered tissues.

Keywords

morphogenesis; mechanobiology; extracellular matrix; fibrin; confocal reflectance; polydimethylsiloxane

Introduction

Mechanical signals are key regulators of cell behavior,[27] and serve as an important link to the extracellular environment. Cells exist in a force-balance between external mechanical inputs and internal, cell-generated traction forces. This “tug-of-war” induces a state of pre-stress in the system, making cells exquisitely sensitive to changes in their mechanical environment.[9] Changes in tissue mechanics are symptomatic of many different pathologies. For example, tumor extracellular matrices are generally much stiffer than surrounding tissues, and tumors often have higher interstitial fluid pressure, both of which alter cell behavior.[1] Increases in stiffness affect the vasculature within a tumor as well,[18] contributing

Corresponding Author: Andrew J. Putnam Department of Biomedical Engineering University of Michigan 2154 Lurie Biomedical Engineering 1101 Beal Avenue Ann Arbor, MI 48109-2110 Telephone: (734) 615-1398 Fax: (734) 647-4834 putnam@umich.edu.

Conflict of Interest Statement
No benefits in any form have been or will be received from a commercial party related directly or indirectly to the subject of this manuscript.

to vessel leakiness and metastasis. Changes in the mechanical microenvironment can contribute to changes in cell behavior, which in turn lead to changes in tissue function.

While such mechanical changes in the microenvironment have been linked with numerous pathologies,[19,5] mechanical stimulation can also be applied to induce desirable changes in cell behavior. Cells not only respond to passive mechanical cues, such as extracellular matrix (ECM) stiffness, but to forces that are actively applied to the matrix, providing a robust way to modify cell behavior. Mechanical stimulation has been shown to improve the integrity of engineered vascular grafts,[10,30] demonstrating the utility of using mechanical signals to improve outcomes. Despite the success of mechanical preconditioning in engineered tissue applications, a better understanding of how the ECM transduces mechanical signals to resident cells might enable the use of applied mechanical forces as a way to control tissue patterning and morphogenesis. Endothelial cell behavior is relatively well characterized in 2D,[28] but it is less clear how strain alters their behavior when challenged to undergo a complex morphogenetic program in 3D, such as angiogenesis.[14,21]

We have developed a system to study the effects of mechanical inputs on angiogenesis by adapting a 3D, microcarrier-based angiogenesis assay, first described by Nehls and Drenckhahn.[25] Human umbilical vein endothelial cells (HUVECs) adhering to gelatin-coated dextran microcarrier beads are embedded in a fibrin matrix and co-cultured with a monolayer of human aortic smooth muscle cells (HASMCs) atop the gel. This 3D culture model is contained with a custom-designed polydimethylsiloxane (PDMS) multi-well platform capable of housing natural and synthetic hydrogels. When clamped into a linear stage, a well-defined static or cyclic uniaxial strain may be applied to the PDMS, which propagates the strain to the ECM and the embedded cells. We show that the application of cyclic strain causes sprouting parallel to the applied strain, and that this biasing is lost if strain is removed. We also show that the observed directional biasing is not simply explained via contact guidance.

Materials and Methods

PDMS Multi-Well Plate and Stretch Device

A PDMS multi-well slab was designed to support 3D cell cultures and to enable them to be subjected to cyclic strain (Fig. 1A). To fabricate the multi-well slab, a Teflon mold was machined to house the PDMS during curing. The wells within the PDMS slab are cubic, 5 mm on a side and spaced 5 mm apart with a 10 mm gap between the end of the outside wells and the edge of the PDMS to facilitate clamping. During strain experiments, the PDMS slab was clamped into a linear stage (Newmark Systems, Mission Viejo, CA) capable of providing precise, reproducible strain (Fig. 1C-E). The clamp apparatus was covered with a lid to improve sterility and a reservoir to keep the semi-open culture system at 100% humidity during cell culture. The reservoir was filled with sterile ddH_2O at the start of the experiment and replenished as necessary. Once the wells of the plate were loaded, the system was placed into a standard cell culture incubator.

Cell Culture

HUVECs were isolated from freshly harvested umbilical cords as previously described.[7] The cords were obtained via a process considered exempt by the University of Michigan's institutional review board because the tissue is normally discarded, and no identifying information is provided to the researchers who receive the cords. Cord veins were flushed with Dulbecco's phosphate-buffered saline (DPBS, Gibco, Carlsbad, CA), then a 0.1% collagenase type 1 (Worthington, Lakewood, NJ) digestion was performed for 15 minutes to release the endothelial cells from the vessel wall. The vessel was flushed with DPBS and the

resulting cell suspension centrifuged, plated, and washed after 24 hours with DPBS to remove any residual erythrocytes. HUVECs were cultured in Endothelial Growth Medium-2 (EGM-2, Lonza, Walkersville, MD) and used at passage 3. Primary HASMCs (Cascade Biologics, Portland, Oregon) were cultured in Medium 231 supplemented with Smooth Muscle Growth Supplement (SMGS, both Invitrogen). HASMCs were used before passage 15. All cell culture was performed in a 37°C, 5.0% CO_2 incubator. Media was changed every other day.

3D Cell Culture and Fibrin Gel Construction

The 3D cell culture model of angiogenesis was modified from previously established protocols.[25,7] Briefly, HUVECs were allowed to attach to gelatin-coated Cytodex® 3 microcarrier beads (Sigma-Aldrich, St. Louis, MO) as follows. HUVECs were trypsinized, pelleted, counted, and 4×10^6 cells were suspended in 5 ml of EGM-2. This suspension was transferred into an upright T-25 culture flask with ten-thousand sterilized microcarrier beads and was gently agitated every 30 minutes. After 4 hours, the suspension was supplied with an additional 5 ml EGM-2 and moved to a fresh T-25, and incubated in normal cell culture position. Coated beads were used within 48 hours.

To create fibrin tissues for 3D cell cultures, 490 μl of 2.5 mg/ml bovine fibrinogen (lot# 029K7636V, Sigma-Aldrich) solutions containing approximately 100 HUVEC-coated microcarrier beads were combined with 10 μl thrombin stock solution (50 U/ml, Sigma-Aldrich). Then, 63 μl of this mixture was quickly transferred into each well of the autoclaved PDMS multi-well plate. Acellular gels used in strain calibration experiments were prepared identically but without microcarrier beads, and with the addition of Fluospheres® Fluorescent Microspheres (1 μm, Red Fluorescent (580/605), Molecular Probes, USA) at a 1:2000 volume ratio. Acellular fibrin gels used for confocal reflectance imaging were created in an identical manner using microcarrier beads with no HUVECs attached. All gels were left at room temperature for 5 minutes to allow the beads to settle to the bottom of the well, and incubated an additional 25 minutes in a 37°C, 5.0% CO_2 incubator to allow for complete gelation. After incubation, 5,000 HASMCs were plated on top of each fibrin gel. Within 30 minutes of plating HASMCs, gels to be used in stretched conditions were clamped into a linear stage and the cyclic strain protocol (10% strain, 0.7 Hz) commenced. PDMS plates cultured statically were placed into petri dishes for sterility. Both strained and static conditions were cultured in a 37°C, 5.0% CO_2 incubator. Media was changed daily for all experiments in PDMS multi-well plates.

Calibration of Strain in 3D Hydrogels

To determine the extent to which the strain applied from the linear motor deformed the fibrin hydrogels embedded within the PDMS slab, 2.5 mg/ml fibrin gels were embedded with Fluospheres® as described above in the PDMS slab and clamped into a custom-built microscope stage insert (Fig. 1B). A micrometer attached to the insert was used to reposition the moving clamp to apply strain to the PDMS slab. Determination of the internal strain in the gel was performed as previously described.[3,17] In short, triads of fluorescent beads randomly distributed within the gel were imaged at 0-12% strain in increments of 2%. Relative distances between these beads at each strain level were used to calculate the first and second principle strains using Lagrangian finite strain analysis (Fig. 2A).

Determination of the Kinetics and Robustness of Directional Sprouting

To determine the effects of cyclic strain on angiogenesis, cell-seeded PDMS multi-well slabs were prepared as described above, divided into static and stretched conditions, and cultured for 5 days. On days 2 through 5, all of the beads within each PDMS slab were imaged.

To determine the robustness of directional sprouting in this system, PDMS multi-well slabs were again prepared. Two slabs were subjected to cyclic strain (Fig. 4A, Groups 1 and 2), while two were left under static conditions initially (Fig. 4A, Groups 3 and 4) for four days. On day 4, plates were imaged. After imaging, one of the previously strained samples was transferred to a static condition, while a previously unstrained PDMS slab was placed in the linear stage and subjected to cyclic strain (Fig. 4A). On day 8, the plates were imaged again. Four experiments were performed for each condition.

Quantification of Network Length and Sprout Angle

Quantification of total network length was performed as described previously.[7] Briefly, vessels from each bead were traced using ImageJ software and summed to determine total network length. For each condition, the network lengths of sprouts coming from 10 individual beads were averaged to determine the total average network length for that condition. To determine the average angle of sprouts coming off of the bead, ImageJ software was used to measure the acute angle of each sprout as it projected from the bead relative to the direction of applied strain (horizontal). Angle measurements from each bead were averaged, followed by averaging of the results across 10 beads to determine the average sprout angle. For all quantifications, 4 independent experiments were performed.

Finite Element Model

To further analyze the local strain within the fibrin gel, a 3D finite element model of the strain field surrounding a single microcarrier bead was created using COMSOL Multiphysics (COMSOL Inc., Burlington, MA). The model assumes 10% uniaxial strain applied to a slab of fibrin gel containing the bead. The fibrin surrounding the bead is modeled as an elastic solid of elastic modulus (E) 3147 Pa, Poisson's ratio (ν) of 0.4992, and density 2.5 mg/ml. The diameter of the bead in the model is 150 μm, which corresponds to the approximate diameter of the Cytodex beads used experimentally (after swelling). The bead is modeled as a rigid solid of modulus 10MPa.

Staining of HUVEC plasma membranes for imaging

To facilitate imaging, HUVEC plasma membranes were stained with the lipophilic carbocyanine SP-DiIC_{18}(3) (Molecular Probes®, Grand Island, NY). Cells were washed once with DPBS, then incubated in DPBS containing 2.5 μM SP-DiIC_{18}(3) at 37°C for 5 minutes, followed by a 15 minute incubation at 4°C to prevent endocytosis of the dye. After the incubation at 4°C, a final DPBS wash was performed, and EGM-2 was replaced.

Confocal Reflectance and Fluorescence Microscopy

Unlabeled fibrin matrices were visualized using confocal reflectance microscopy. Confocal reflectance images were taken on a Zeiss LSM 510-META Laser Scanning Confocal microscope using a 63x water immersion objective (C-Aprochromat, Carl Zeiss, Thornwood, NY). Fibrin gels were illuminated using a 488 nm Argon laser through an 80/20 filter. Other fluorescence images were taken on an Olympus IX81 microscope equipped with a 100-W high pressure mercury lamp (Olympus, Center Valley, PA) and Hammamatsu camera (Bridgewater, NJ). Quantification of fiber alignment in the confocal reflectance images was carried out as follows. The Fast-Fourier Transform (FFT) process in NIH ImageJ software was used to generate new image in the frequency space, in which each pixel represents a vector whose position is determined by the direction of a particular periodic structure in the spatial domain of the image. To provide a quantitative metric of fiber orientation, radial sums of pixel intensity were calculated from the FFT images using the Oval Profile add-on in ImageJ.

Statistical Analysis

Statistical analysis was performed using open source R software (www.r-project.org). Two-way analysis of variance (ANOVA) was performed and pairwise comparisons were made using Tukey's method. The threshold for statistical significance was set at $p < 0.05$. Data are reported as mean ± SEM.

Results

Quantification of microscale strain confirms that strain applied to the PDMS propagates into the fibrin gel

The first step in this study was to confirm that strain applied to the PDMS slab was propagated into the fibrin, and to subsequently calibrate the measured strain with the applied strain. To accomplish this goal, red fluorescent microcarrier beads were embedded in the fibrin gels. Displacements of the microspheres under strain (0-12%) were measured, revealing that the first principle strain in the system responded linearly ($R^2 = 0.9297$) to the applied strain (Fig. 2B). The second principle strain, a metric of strain in the direction orthogonal to the applied strain, showed a weaker, but still linear ($R^2 = 0.5336$), negative trend with increasing applied strain (Fig. 2C). These calibration results show that uniaxial strain applied to the PDMS slab propagates into the fibrin gels in our system.

Cyclic strain alters the direction, but not the magnitude, of angiogenic sprouting

Following calibration, we used our mechanical strain device to apply cyclic strain (10% strain, 0.7 Hz) to the 3D fibrin-based model of angiogenesis. This regimen was chosen to conform with published experiments showing directional alignment in 3D assays.[31,16,21] Representative images of capillaries formed under static and strained conditions, respectively (Fig. 3A-B), reveal clear differences in capillary sprouting in strained versus control cultures. (Constructs lacking HASMCs or other similar stromal cell type fail to form capillary-like networks within this system in our hands; Supplemental Figure 1.) No statistically significant differences in average total network lengths were observed between the strained and static conditions on days 2-5 (Fig. 3C). However, significant differences were observed in sprouting direction. By day 2, the static cultures contained capillary sprouts with an average sprout angle of 39.9±7.1°, showing nearly perfectly random radial outward growth from a bead (Fig. 3D). In contrast, cells in the strained cultures yielded capillary sprouts with an average sprout angle of 29.7±4.2°, significantly lower ($p < 0.05$) than that for the static cultures (Fig. 3D).

Direction of angiogenic sprouting is sensitive to changes in strain regimen

In order to test the stability of the directional biasing, four experimental groups were created (Fig. 4A). The magnitude of capillary sprouting was not significantly different across any of these four groups at day 4 or 8 (Fig. 4B), consistent with the data presented earlier (Fig. 3C). By contrast, there were significant adjustments in sprout angle when the strain regimen was altered. Image analysis revealed that the conditions with constant regimens [i.e., the condition cultured under strain for 8 days (Group 1) and the condition cultured statically for 8 days (Group 4)] showed no changes in the angle of capillary sprouting between days 4 and 8, as expected. The condition that was cultured statically for 4 days then cyclically strained for 4 days (Group 3) showed a slightly negative, but not statistically significant, change in sprout angle at day 8. In contrast, however, the condition that was strained for 4 days then cultured statically for 4 days (Group 2) showed a complete loss of directional biasing, with sprouts growing radially outward from the bead at day 8.

Matrix architecture shows only modest changes due to the applied strain

Confocal reflectance images of the angiogenesis assay, taken under static conditions on days 2-5, showed significant remodeling of the extracellular matrix caused by the invading endothelial cells, but no visible alignment of fibrin fibers (Fig. 5A-H). To examine the strain field surrounding a microcarrier bead, a 3D finite element model was generated, and the strain distributions in the x-y (Fig. 6A) and x-z (Fig. 6B) assessed. Under an applied strain of 10%, the x-y plane shows 10% first principle strain throughout the gel, as well as distortions to the strain field surrounding the embedded microcarrier. Near the regions of the bead normal to the applied strain, the simulation shows strains increasing to approximately 17%; by contrast, near the regions of the bead tangential to the applied strain, the simulation shows strains of approximately 6%. These data suggest that the microcarrier beads themselves can both slightly amplify and slightly dampen the applied strain, depending on the face of the bead considered. The x-z plane shows similar characteristics as the x-y plane, with strain damping observed in the positive z-direction with respect to the bead (perpendicular to the strain direction), and amplification in the positive and negative x-directions. This prediction is expected since our system applies a uniaxial strain in the x-direction.

Confocal reflectance images of acellular fibrin gels containing microcarriers, but no cells, were taken to complement the finite element model (Fig. 6C, D, F, G). When imaged under 10% strain, only modest alignment (at best) of the fibrin fibers parallel to the direction of strain was observed (Fig. 6C-D, strain direction is horizontal) when visually compared to the unstrained conditions (Fig. 6F-G). Reflectance pictures of acellular gels containing no beads (Fig. 6E,H) showed no visual difference in fiber alignment between strained and unstrained conditions.

To further characterize the orientation of the fibers under static and strained conditions, Fourier transforms of the images in Figures 6D and G were generated and analyzed using NIH ImageJ (Fig. 6I, J). Computed intensity values for each angle represent the degree of fiber orientation in the image at that angle. Results normalized to the raw values computed at zero degrees in each image show slight peaks in intensity at 0, 180, and 360 degrees, indicating some possible alignment of the fibers in the horizontal direction; however, there were no significant differences in these peaks between the static and strained conditions.

Discussion

In this study, we developed and characterized a custom-made mechanical strain device that supports a 3D co-culture model of angiogenic sprouting widely used in the literature.[7,25,26,31] With this new device, we showed here that cyclic strain applied to endothelial cells in a 3D hydrogel controls angiogenic pattern formation. Specifically, cyclic strain promoted alignment parallel to the direction of strain when the strain regimen was initiated at the beginning of the culture period. Moving strained samples to a static environment caused a randomization of sprout angle, implying that the direction of sprouting does have a degree of plasticity even after vessels have formed. Applying cyclic strain to the cultures after vessel-like structures had already formed induced a slight change in the subsequent sprouting direction as well, but the change was not quite statistically significant. However, the challenge of accurately measuring changes in capillary orientation in a pre-formed network without a fixed starting point may have contributed to an increased measurement uncertainty in this particular condition.

The results of our study here add to the growing body of evidence that collectively supports the idea that applied mechanical forces can direct the formation of capillary networks. However, consensus has not been reached as to whether mechanical forces positively or

negatively influence vessel growth due to many contradictory studies. For example, Kilarski, et al. showed that forces generated by endogenous fibroblasts promote the development and growth of new vessels during wound healing *in vivo*.[12] By contrast, Boerckel, et al. recently showed that externally applied mechanical loads can actually reduce vessel invasion in a bone injury model when applied at early time points, while enhancing vascular remodeling when the load is applied after a delay.[4] Our quantitative data here show that ECs subjected to cyclic strain form capillary networks to the same extent as those cultured in static conditions, similar to a study by Krishnan, et al. which found no differences in segment length distribution in strained and unstrained collagen gels.[16] Beyond the magnitude of capillary sprouting, there are also contradictory publications with respect to the influence of applied strain on directionality. Our observation that capillary sprouting occurs parallel to the direction of applied strain is consistent with the Krishnan, et al. study in which new sprouts initiated from isolated microvessels embedded in 3D collagen gels aligned parallel to the direction of applied cyclic strain (6% strain, 1 Hz).[16] However, a study using a similar microcarrier-based model system reported sprouting in a direction perpendicular to the applied cyclic strain.[21]

In order to put our results in the context of these earlier studies, it is important to understand two key differences with respect to our model system and data. First, our model system contains a monolayer of smooth muscle cells on top of the fibrin gel. In prior studies using our model, we have found that some type of stromal cell is essential to stimulate the ECs to form robust capillary-like structures with hollow, well-defined lumens.[13,8] Experiments with ECs alone did not induce alignment perpendicular to the applied strain in our system, but instead compromised the formation of sprouts altogether (Supplemental Figure 1). Other groups have attempted to characterize the complex milieu of factors supplied by the interstitial cells, confirming the requirement for an interstitial cell type to be present for angiogenesis,[24] and showing that certain factors are required for lumen formation (e.g. soluble collagen 1),[26] but the precise combination of factors for production of mature capillaries in this system remains unknown. Given that the aim of this work is to assess the effects of strain on angiogenesis, we utilized a co-culture system known to facilitate robust angiogenesis in spite of any possible confounding factors.

A second important distinction of our findings is our data showing that cyclic strain did not significantly align the fibrin matrix, at least as detected via confocal reflection microscopy. On one hand, this finding is consistent with those of Matsumoto, et al., who showed that cyclic strain of 7% amplitude did not induce any perceptible alignment of fibrin fibrils.[20] On the other hand, Korff and Augustin showed that ECM alignment in response to EC-generated tensile forces caused directional sprouting.[14] A more recent study showed that endothelial sprouting from spheroids occurred in a directional fashion in fibrin gels that had been aligned via an applied magnetic field or EC-generated forces.[23] In our model system, the mechanism by which applied strain induced directional alignment of the capillary-like networks is not simply explained by ECM realignment and contact guidance. The randomization of capillary sprouting after the strain is removed further supports this statement, and implies that any subtle strain-induced local anisotropies in matrix architecture are not permanent.

While we cannot rule out that subtle ECM realignment may play a role in directional capillary sprouting in our system, an alternative explanation is that the applied strain may induce local changes in ECM stiffness, without significantly disrupting fiber architecture. A previous study has shown that fibrin begins to exhibit strain stiffening at approximately 10% strain, and that this stiffening occurs before fiber alignment can be detected by birefringence.[11] Matrix alignment itself can also increase the apparent stiffness of the ECM in the direction of alignment,[29] but any potential change in local fibrin mechanics here in

our study occurred independently of matrix alignment. Local matrix anisotropy is difficult to measure and therefore possible local matrix strain stiffening is rarely examined. To address the question of how strain affects local matrix mechanics and cell behavior, Kotlarchyk et al. showed that applied strain induces local changes to fibrin stiffness in 3D gels, leading to differential cell behavior in regions of different stiffness.[15] Our finite element results showing strain amplification on the face of the bead normal to the strain direction agree with previous work showing that a rigid inclusion on a deformable membrane,[22] as well as in a fibrin gel,[2] can cause strain amplification in the vicinity of the inclusion. Thus, strain amplification around the microcarriers (and also at rigid boundaries) may cause substantial strain, and stiffness, gradients.

Our finite element model assumes a no-slip condition between the microcarrier and the fibrin gel, which we believe is a valid assumption for two reasons. First, in the biological assay the microcarriers are coated with endothelial cells, which are attached to the gelatin-coated bead as well as the outlying fibrin matrix through their integrin receptors. These integrin attachments provide a continuous mechanical linkage between the fibrin gel and the underlying microcarrier. Second, the confocal reflectance images of beads under strain in Figure 6 show that, even in acellular gels, there appears to be no physical separation between the microcarrier and the fibrin gel under the strain conditions used in this study.

Our data show that cyclic strain can be used to produce directional capillary growth during angiogenesis without a diminishing the extent of network formation, which is encouraging from a tissue engineering perspective. It has already been established that the implantation of a pre-vascularized tissue improves the rate of anastomosis with the host vasculature,[6] an important factor in the survival of large tissue implants. Pre-vascularization and alignment may therefore represent a viable strategy to nourish metabolically active engineered tissues that also require alignment to function properly, such as cardiac muscle tissue. An improved understanding of the mechanical environment surrounding cells undergoing complex morphogenetic programs may illuminate the engineering parameters necessary to create large, implantable tissues. Finally, we highlight an interaction between a tissue and a rigid boundary, providing insight into the interaction between implanted medical devices and the surrounding vasculature. In light of the modeling data presented here and the pronounced angiogenic response surrounding a microcarrier bead, understanding the mechanical environment surrounding an implant is necessary to effectively combat, or take advantage of, the host response.

Supplementary Material

Refer to Web version on PubMed Central for supplementary material.

Acknowledgments

The authors acknowledge Rahul Singh for providing data for the finite element model and Stephanie Grainger for helpful discussions. This work was supported by grants R01-HL085339 and R01-HL085339-S1 from the NIH.

References

1. Baker EL, Bonnecaze RT, Zaman MH. Extracellular matrix stiffness and architecture govern intracellular rheology in cancer. Biophys J. 2009; 97:1013–1021. [PubMed: 19686648]
2. Balestrini JL, Skorinko JK, Hera A, Gaudette GR, Billiar KL. Applying controlled non-uniform deformation for in vitro studies of cell mechanobiology. Biomechanics and modeling in mechanobiology. 2010; 9:329–344. [PubMed: 20169395]
3. Barbee KA, Macarak EJ, Thibault LE. Strain measurements in cultured vascular smooth muscle cells subjected to mechanical deformation. Ann Biomed Eng. 1994; 22:14–22. [PubMed: 8060022]

4. Boerckel JD, Uhrig BA, Willett NJ, Huebsch N, Guldberg RE. Mechanical regulation of vascular growth and tissue regeneration in vivo. Proceedings of the National Academy of Sciences of the United States of America. 2011; 108:E674–680. [PubMed: 21876139]
5. Cecchi E, Giglioli C, Valente S, Lazzeri C, Gensini GF, Abbate R, Mannini L. Role of hemodynamic shear stress in cardiovascular disease. Atherosclerosis. 2011; 214:249–256. [PubMed: 20970139]
6. Chen X, Aledia AS, Ghajar CM, Griffith CK, Putnam AJ, Hughes CC, George SC. Prevascularization of a fibrin-based tissue construct accelerates the formation of functional anastomosis with host vasculature. Tissue engineering. Part A. 2009; 15:1363–1371. [PubMed: 18976155]
7. Ghajar CM, Blevins KS, Hughes CC, George SC, Putnam AJ. Mesenchymal stem cells enhance angiogenesis in mechanically viable prevascularized tissues via early matrix metalloproteinase upregulation. Tissue engineering. 2006; 12:2875–2888. [PubMed: 17518656]
8. Ghajar CM, Kachgal S, Kniazeva E, Mori H, Costes SV, George SC, Putnam AJ. Mesenchymal cells stimulate capillary morphogenesis via distinct proteolytic mechanisms. Experimental cell research. 2010; 316:813–825.
9. Ingber DE. Mechanical signaling and the cellular response to extracellular matrix in angiogenesis and cardiovascular physiology. Circ Res. 2002; 91:877–887. [PubMed: 12433832]
10. Jeong SI, Kwon JH, Lim JI, Cho SW, Jung Y, Sung WJ, Kim SH, Kim YH, Lee YM, Kim BS, Choi CY, Kim SJ. Mechano-active tissue engineering of vascular smooth muscle using pulsatile perfusion bioreactors and elastic plcl scaffolds. Biomaterials. 2005; 26:1405–1411.
11. Kang H, Wen Q, Janmey PA, Tang JX, Conti E, MacKintosh FC. Nonlinear elasticity of stiff filament networks: Strain stiffening, negative normal stress, and filament alignment in fibrin gels. The journal of physical chemistry. B. 2009; 113:3799–3805. [PubMed: 19243107]
12. Kilarski WW, Samolov B, Petersson L, Kvanta A, Gerwins P. Biomechanical regulation of blood vessel growth during tissue vascularization. Nature medicine. 2009; 15:657–664.
13. Kniazeva E, Putnam AJ. Endothelial cell traction and ecm density influence both capillary morphogenesis and maintenance in 3-d. American journal of physiology. Cell physiology. 2009; 297:C179–187. [PubMed: 19439531]
14. Korff T, Augustin HG. Tensional forces in fibrillar extracellular matrices control directional capillary sprouting. J Cell Sci. 1999; 112(Pt 19):3249–3258. [PubMed: 10504330]
15. Kotlarchyk MA, Shreim SG, Alvarez-Elizondo MB, Estrada LC, Singh R, Valdevit L, Kniazeva E, Gratton E, Putnam AJ, Botvinick EL. Concentration independent modulation of local micromechanics in a fibrin gel. PLoS One. 2011; 6:e20201. [PubMed: 21629793]
16. Krishnan L, Underwood CJ, Maas S, Ellis BJ, Kode TC, Hoying JB, Weiss JA. Effect of mechanical boundary conditions on orientation of angiogenic microvessels. Cardiovascular research. 2008; 78:324–332. [PubMed: 18310100]
17. Lee AA, Delhaas T, Waldman LK, MacKenna DA, Villarreal FJ, McCulloch AD. An equibiaxial strain system for cultured cells. Am J Physiol. 1996; 271:C1400–1408. [PubMed: 8897847]
18. Lopez JI, Kang I, You WK, McDonald DM, Weaver VM. In situ force mapping of mammary gland transformation. Integrative biology : quantitative biosciences from nano to macro. 2011; 3:910–921. [PubMed: 21842067]
19. Malek AM, Alper SL, Izumo S. Hemodynamic shear stress and its role in atherosclerosis. JAMA. 1999; 282:2035–2042. [PubMed: 10591386]
20. Matsumoto T, Sasaki J, Alsberg E, Egusa H, Yatani H, Sohmura T. Three-dimensional cell and tissue patterning in a strained fibrin gel system. PLoS One. 2007; 2:e1211. [PubMed: 18030345]
21. Matsumoto T, Yung YC, Fischbach C, Kong HJ, Nakaoka R, Mooney DJ. Mechanical strain regulates endothelial cell patterning in vitro. Tissue Eng. 2007; 13:207–217. [PubMed: 17518594]
22. Mori D, David G, Humphrey JD, Moore JE Jr. Stress distribution in a circular membrane with a central fixation. Journal of biomechanical engineering. 2005; 127:549–553. [PubMed: 16060363]
23. Morin KT, Tranquillo RT. Guided sprouting from endothelial spheroids in fibrin gels aligned by magnetic fields and cell-induced gel compaction. Biomaterials. 2011; 32:6111–6118. [PubMed: 21636127]

24. Nakatsu MN, Sainson RC, Aoto JN, Taylor KL, Aitkenhead M, Perez-del-Pulgar S, Carpenter PM, Hughes CC. Angiogenic sprouting and capillary lumen formation modeled by human umbilical vein endothelial cells (huvec) in fibrin gels: The role of fibroblasts and angiopoietin-1. Microvascular research. 2003; 66:102–112. [PubMed: 12935768]
25. Nehls V, Drenckhahn D. A novel, microcarrier-based in vitro assay for rapid and reliable quantification of three-dimensional cell migration and angiogenesis. Microvascular research. 1995; 50:311–322. [PubMed: 8583947]
26. Newman AC, Nakatsu MN, Chou W, Gershon PD, Hughes CC. The requirement for fibroblasts in angiogenesis: Fibroblast-derived matrix proteins are essential for endothelial cell lumen formation. Molecular biology of the cell. 2011; 22:3791–3800. [PubMed: 21865599]
27. Peyton SR, Ghajar CM, Khatiwala CB, Putnam AJ. The emergence of ecm mechanics and cytoskeletal tension as important regulators of cell function. Cell Biochem Biophys. 2007; 47:300–320. [PubMed: 17652777]
28. Thodeti CK, Matthews B, Ravi A, Mammoto A, Ghosh K, Bracha AL, Ingber DE. Trpv4 channels mediate cyclic strain-induced endothelial cell reorientation through integrin-to-integrin signaling. Circ Res. 2009; 104:1123–1130. [PubMed: 19359599]
29. Tranquillo RT, Durrani MA, Moon AG. Tissue engineering science: Consequences of cell traction force. Cytotechnology. 1992; 10:225–250. [PubMed: 1369238]
30. Yazdani SK, Tillman BW, Berry JL, Soker S, Geary RL. The fate of an endothelium layer after preconditioning. J Vasc Surg. 2010; 51:174–183. [PubMed: 20117500]
31. Yung YC, Chae J, Buehler MJ, Hunter CP, Mooney DJ. Cyclic tensile strain triggers a sequence of autocrine and paracrine signaling to regulate angiogenic sprouting in human vascular cells. Proceedings of the National Academy of Sciences of the United States of America. 2009; 106:15279–15284. [PubMed: 19706407]

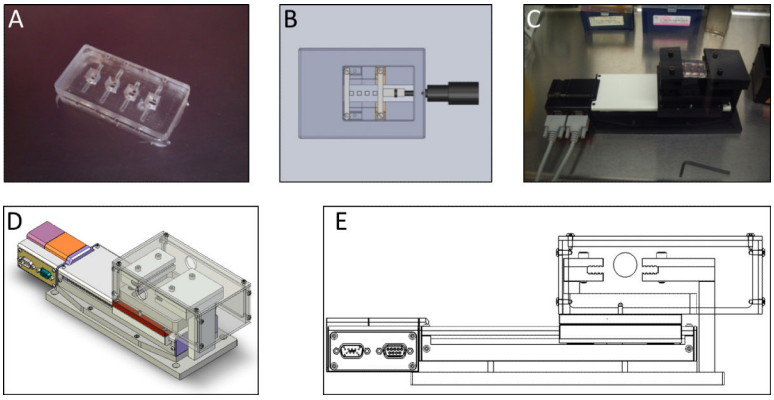

Figure 1.

Devices used to house and apply strain to hydrogels. **A.** PDMS multi-well plate. **B.** Schematic of microscope stage insert used for calibration of micro-scale strain. **C-E.** Linear stage used to apply cyclic strain to PDMS multi-well plate.

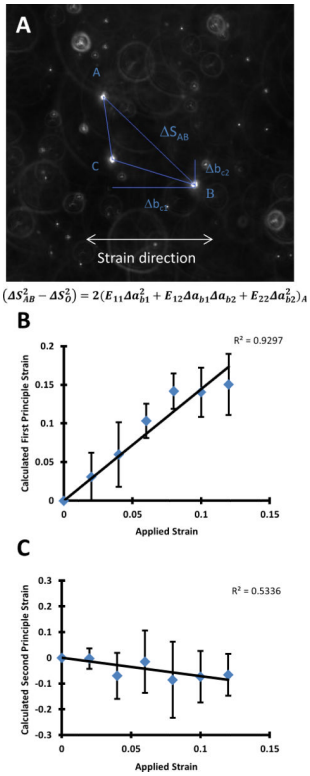

Figure 2.

Relationship between applied strain and strain within the fibrin gel. **A.** Representative image of a triad used in strain calibration. A system of equations was solved for E_{11}, E_{12}, and E_{22}, which were used to calculate the principle strains. Shown are the first (**B.**) and second (**C.**) principle strains within the fibrin matrix. 15 triads were used for this analysis.

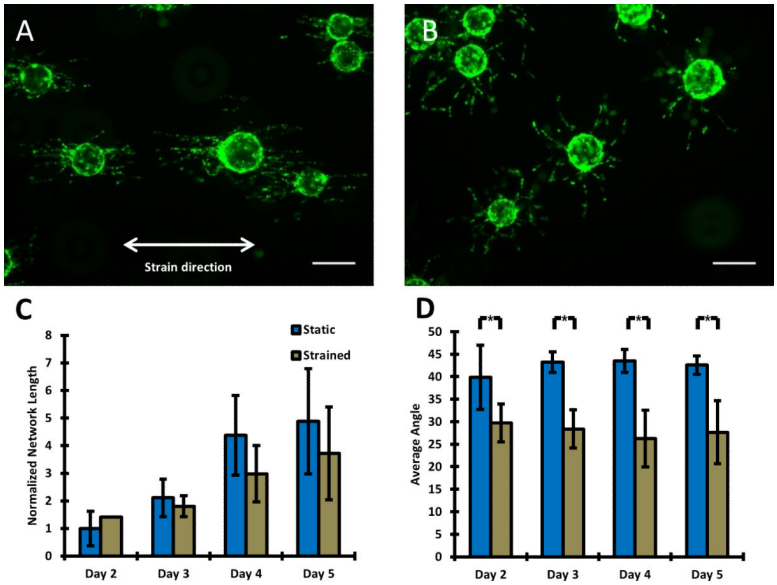

Figure 3.

Effects of cyclic strain on angiogenesis. **A-B.** Representative pictures of HUVEC-coated dextran microcarrier beads at day 5 in 3D angiogenesis assay under strained (left) and static (right) conditions. **C.** Normalized network lengths of strained and unstrained capillaries. Data for each condition were normalized to the day 2 unstrained condition. No significant differences were observed between the strained and unstrained conditions at each time point. **D.** A significant decrease in average sprout angle was observed in the strained conditions (relative to unstrained) for all time points. Random alignment corresponds to an average angle of 45 degrees, while perfect alignment in the direction of strain corresponds to 0 degrees. Data reported as mean +/− S.E.M. Scale bars 100 microns.

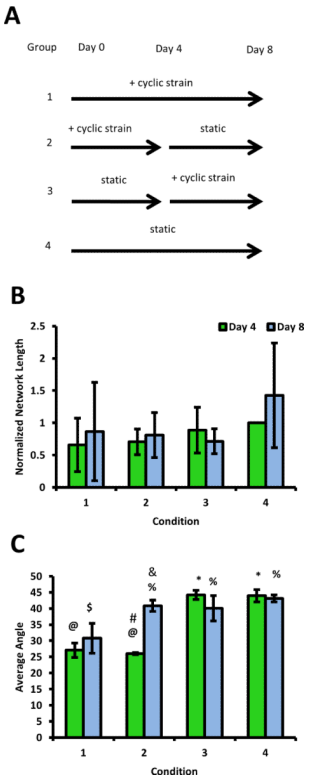

Figure 4.

Effects of a change in strain regimen on angiogenesis. **A.** Schematic depicting the four different experimental groups, each of which was quantified for total network length and average sprout angle on day 4 and day 8. Strained conditions were subjected to 10% strain, 0.7Hz. **B.** Quantification of network lengths, normalized to the day 4 unstrained condition, showed that the magnitude of sprouting was unaffected by changes in the strain regimen. **C.** Cells under strain showed biasing parallel to the direction of strain at day 4. When the strain stimulus was removed, biasing disappeared. @ and * are statistically different, $ and % are statistically different, # and & are statistically different. Other comparisons are either not significant or were not made. Random alignment corresponds to an average angle of 45 degrees, while perfect alignment in the direction of strain corresponds to 0 degrees. Data reported as mean +/− S.E.M.

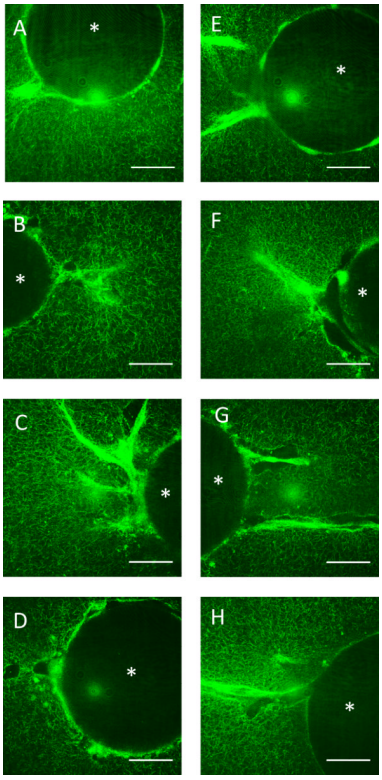

Figure 5.
Confocal reflectance images of the fibrin matrix at days 2-5 of the angiogenesis assay. **A,E.** Day 2, **B,F.** Day 3, **C,G.** Day 4 **D,H.** Day 5 of the microcarrier bead angiogenesis assay. **A-D.** Static conditions, **E-H.** Stretched conditions. The asterisk in each image denotes the microcarrier bead. Images pseudo-colored green for clarity. Scale bars = 50 μm.

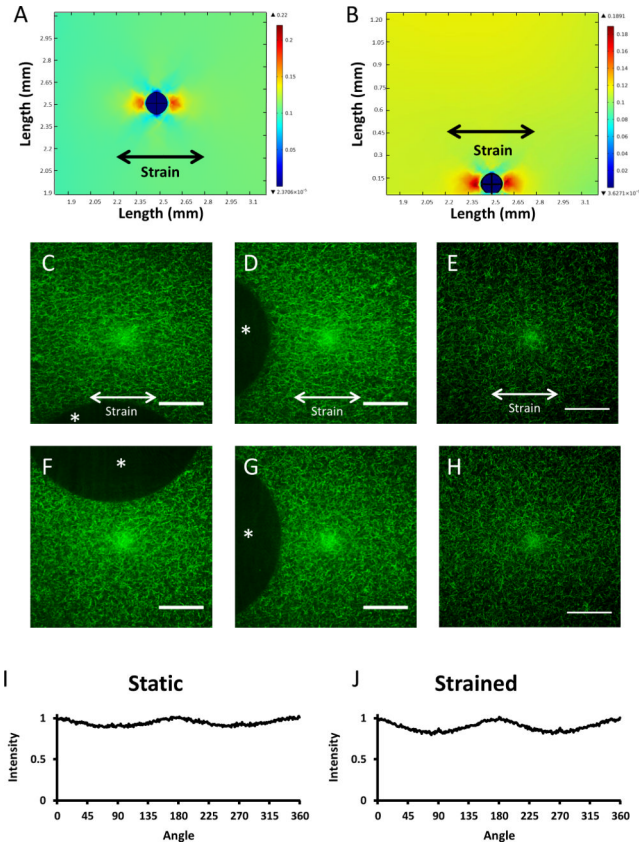

Figure 6.

The effects of strain on ECM architecture. A-B. Linear elastic models of a fibrin hydrogel containing a microcarrier bead and subjected to 10% strain. In both the x-y (A) and x-z (B) planes, strain is amplified on the left and right faces of the bead, normal to the applied strain; strain is damped on the faces tangential to the applied strain. C, D, F, G. Confocal reflectance images of fibrin matrix surrounding a strained bead show modest fiber alignment when the gel is strained 10% (C,D) and random orientation when static (F,G). The asterisk in each image denotes the microcarrier bead. There appear to be no differences in matrix architecture far from any boundary condition in the strained (E) and unstrained (H) conditions. FFT Analysis (I, J) of images D and G shows a similar degree of fiber alignment in the strained and static conditions in the horizontal direction, with moderate peaks at 0, 180, and 360 degrees. Strain direction is horizontal. Images pseudo-colored green for clarity. Scale bars = 50 μm.